Driving Forces of Conformational Changes in Single-Layer Graphene Oxide

Raymond L. D. Whitby,[†,*] Vladimir M. Gun'ko,[‡] Alina Korobeinyk,[†] Rosa Busquets,[†] Andrew B. Cundy,[†] Krisztina László,[§] Jadwiga Skubiszewska-Zięba,[⊥] Roman Leboda,[⊥] Etelka Tombácz,[¶] Ildiko Y. Toth,[¶] Krisztina Kovacs,[¶] and Sergey V. Mikhalovsky[†,∥]

[†]Nanoscience & Nanotechnology Group, Faculty of Science and Engineering, University of Brighton, Lewes Road, Brighton, BN2 4GJ, United Kingdom, [‡]Chuiko Institute of Surface Chemistry, 17 General Naumov Street, 03164 Kiev, Ukraine, [§]Budapest University of Technology and Economics, H-1521 Budapest, Hungary, [⊥]Maria Curie-Skłodowska University, 20031 Lublin, Poland, [¶]Department of Physical Chemistry and Material Science, University of Szeged, H-6720 Szeged, Hungary, and [∥]Nazarbayev University, Astana, 010000, Kazakhstan

ABSTRACT

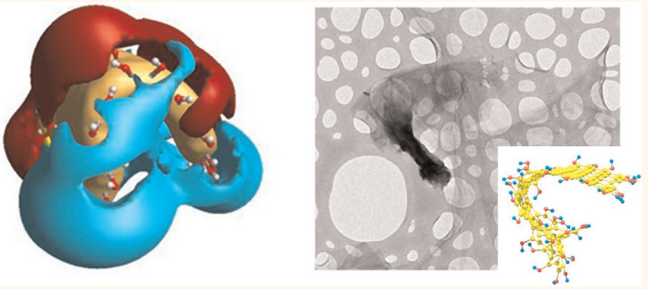

The extensive oxygen-group functionality of single-layer graphene oxide proffers useful anchor sites for chemical functionalization in the controlled formation of graphene architecture and composites. However, the physicochemical environment of graphene oxide and its single-atom thickness facilitate its ability to undergo conformational changes due to responses to its environment, whether pH, salinity, or temperature. Here, we report experimental and molecular simulations confirming the conformational changes of single-layer graphene oxide sheets from the wet or dry state. MD, PM6, and *ab initio* simulations of dry SLG and dry and wetted SLGO and electron microscopy imaging show marked differences in the properties of the materials that can explain variations in previously observed results for the pH dependent behavior of SLGO and electrical conductivity of chemically modified graphene-polymer composites. Understanding the physicochemical responses of graphene and graphene oxide architecture and performing selected chemistry will ultimately facilitate greater tunability of their performance.

KEYWORDS: graphene · conformation changes · surface reactivity · structural modeling · pH changes

The effect of the chemical environment on the architecture of single-layer graphene (SLG) or its oxide derivative (SLGO) is important when considering its possible applications as a polymer strengthening agent,[1] in heterogeneous catalysis,[2] manipulation of electrical conductivity,[3] drug delivery,[4] or wastewater cleanup.[5] The ability of graphene sheets to change their morphology under the influence of chemical factors is also an example of converting chemical energy into mechanical energy, which may have interesting applications. A variety of graphene structures have been observed from folding to bending to scrolling,[6−9] yet the influence of chemical environment over the final morphology of SLGO is poorly understood.

Quantum chemical and molecular dynamic simulations of SLG have revealed that individual sheets, ribbons, and scrolls can spontaneously change conformation.[10] However, these simulations did not account for the extensive oxygen functionality that is systemic for SLGO produced from chemically expanded and exfoliated graphite. The stability of aqueous SLGO suspensions is determined by several factors such as the hydration of the oxygen-containing groups, the negative surface charge (due to the reaction: $-COOH(s) \rightarrow -COO^-(s) + H^+(aq)$) causing intersheet repulsion,[11] and the hydration of hydrophobic fragments. In contact with cations, the negative charge can be overcome causing precipitation of SLGO from its suspension, known as salting out.

Molecular dynamics simulations have been performed for graphene oxide sheets in order to study their aggregation at different pH values; the surface energy of SLGO was calculated from the charging of oxygen-containing functional groups decorating the periphery and the surface of graphene. The model used was deliberately functionalized with a low degree of carboxylic, hydroxyl, and epoxy groups randomly attached to the SLGO sheets, but the small sheet area was

* Address correspondence to r.whitby@brighton.ac.uk.

Received for review January 16, 2012 and accepted April 11, 2012.

Published online April 11, 2012
10.1021/nn3002278

insufficient to generate conformational changes.[12] Here, we use a combination of experimental data and molecular simulations to reveal the chemically driven mechanism of morphology changes of SLG and SLGO functionalized with oxygen-containing groups in response to its chemical environment.

RESULTS AND DISCUSSION

The stability of aqueous SLGO suspensions at various pH was examined following their purification with an alkali solution to remove oxidative debris (Supporting Information). The increase in pH of the chemical environment leads to deprotonation of acidic functional groups as in the reaction: $-COOH(s) + OH^-(aq) \rightarrow -COO^-(s) + H_2O$ and the zeta potential of SLGO drops from −20 mV to −45 mV with pH increasing from 2 to 11, respectively (Figure S1 in the Supporting Information). This corresponds to the negative surface charge density uncompensated by counterions in the shear layer (a compacted part plus a part of the diffuse layer of the electrical double layer, EDL). As expected, the aqueous SLGO suspension becomes unstable when the zeta potential increases above −30 mV at around pH 3, due to reduced electrostatic repulsion, which can be observed by the instant precipitation of SLGO (Figure S1 insert).

It was found that the conformation of SLGO can be significantly affected by pH; at low pH SLGO exists predominantly as flat sheets with a high degree of agglomeration between the sheets, but at higher pH (>7) the SLGO sheets begin to collapse (Figure 1a−c).[13] The conformational changes may explain the presence of a small hysteresis loop detected in potentiometric titrations (Figure 1d), which weakly depends on the ionic strength of the solution in the range from 0.005 to 0.5 M KCl. It has also been found that the drying of SLGO from solvents (particularly water) exerts surface tension effects on the graphitic domains; this behavior is similar to carbon nanotube systems under drying,[14] which may exacerbate folding effects. However, the type of intrasheet collapse that occurs at high pH (>7, Figure 1c) was not observed at low pH (<7, Figure 1a), which justifies the inferred pH-dependence mechanism.

Three types of calculations (*ab initio*, PM6, and MD/CharMM) applied here to different SLGO and SLG models (from 220 to 13000 atoms) were utilized to examine effects of oxygen functionality on the graphene geometry changes. The PM6/MOZIME[15] calculations of unfolded and folded SLGO sheets, with randomly distributed O-containing functionalities, show that the formation of strongly bent SLGO structures (Figure 2c,e) is more favorable than flat sheets (Figure 2a). In these calculations the ratio between carboxylic, lactone, and phenolic functional groups matched the acid−base (Boehm) titration analysis data with a total of ∼6 atom % of O atoms in the sheet.[16] A large rectangular ∼21 nm by ∼8 nm sheet has been used for both SLG and SLGO calculations (Figure 2). CharMM force field calculations of this sheet and two- or 4-fold smaller sheets (*ca.* 5−10 nm), hydrated and nonhydrated, revealed a stronger tendency for unfolding for smaller structures. The *ab initio* (HF/6-31G(d,p)) calculations of small SLGO models (Figure 3) show only little bending of an oxidized part of the sheet, but a nonoxidized part is practically planar. Herein, a number of in-plane lattice vacancies (Figure 2a) were introduced to the SLGO structure and terminated with oxygen-containing groups in order to reflect the sheet-etching process of the basal planes during the acid oxidation process.[17] The difference between the total energy of bent and planar SLGO structures (e) and (a), $\Delta E_t = E_{t,e} - E_{t,a} = -1021$ kJ/mol (PM6). The strongly bent SLGO structure (Figure 2c), which was first calculated with the CharMM force field and then optimized by PM6/MOZYME to reach small energy gradient values corresponding to a local minimum at the potential energy surface, has a higher energy than less tightly folded (Figure 2e) and planar (Figure 2a) structures ($E_{t,c} - E_{t,a} = 1250$ kJ/mol). However, for the SLG model the difference between the total energy of a bent structure (Figure 2f) and a flat sheet (Figure 2b) is positive $\Delta E_t =$ 2017 kJ/mol, which indicates that the planar SLGO structure (Figure 2a) is less stable than bent SLGO (Figure 2e), and SLG is more stable in a flat conformation (Figure 2b). The radius of curvature is larger for bent SLG (Figures 2d,f) than that for SLGO (Figures 2c,e) because of the intrasheet defects in the latter. However, the spacing between neighboring fragments in the bent SLG is smaller (Figure 2d) (0.39 nm, close to that in graphite stacks, 0.34−0.38 nm) than in SLGO (0.42 nm) due to the presence of O-containing functionalities which increase roughness of the defect-laden SLGO sheets in comparison with flat defect-free SLG sheets. Somewhat counterintuitively, this gap between fragments does not disappear during the unfolding of bent SLGO and SLG since one surface "slides" along the second surface. The spacing value in the bent SLGO model corresponds to the spacing peak calculated from the XRD data for SLGO dried from suspension at pH 1 (causing a low surface charge density) or a shoulder in the distribution function for SLGO dried from suspension at pH 14 (with maximum surface charging) (Supporting Information, Figure S4).

The conformational changes of a graphene sheet can be conveniently visualized using the field point method.[18] Although all interactions in a molecule are electrostatic in their origin, the whole electrostatic field surrounding the molecule can be broken down into four types of interactions, or fields, which correspond to (i) predominantly hydrophobic interactions, (ii) van der Waals attraction forces, or electrostatic fields dominated by (iii) electropositive or (iv) electronegative

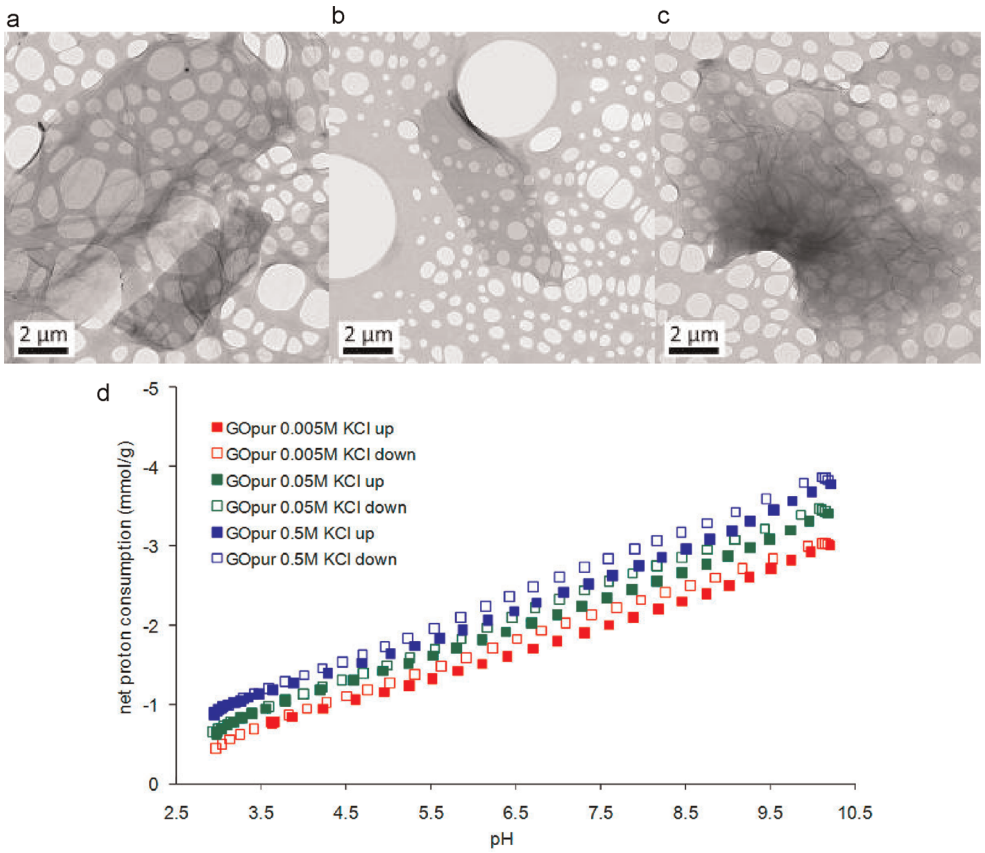

Figure 1. TEM images of SLGO at pH (a) 5, (b) 7, and (c) 9, in 10 mM buffered solutions; (d) pH-dependent protonation and deprotonation of acidic functionalities on SLGO measured by cyclic titration in the direction of increasing (up) and decreasing (down) pH at different ionic strengths.

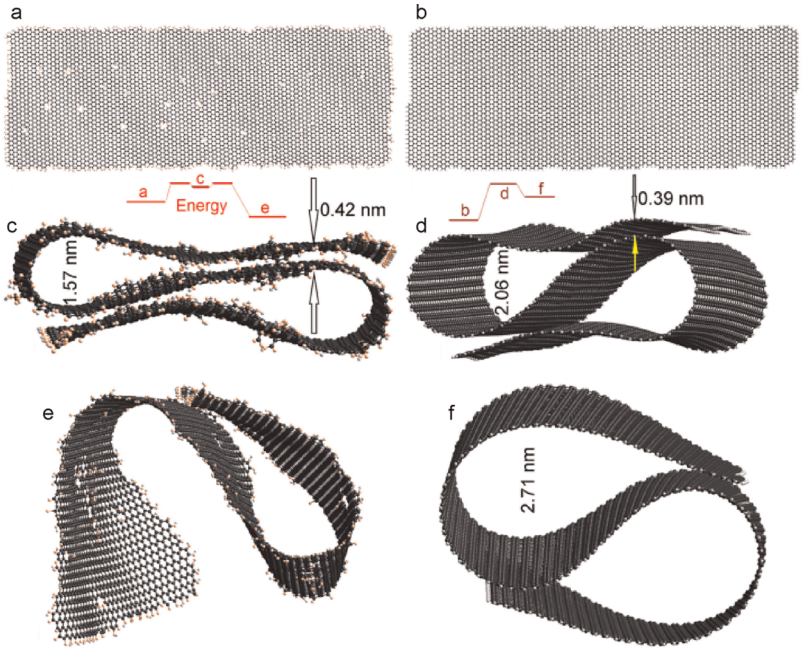

Figure 2. Model sheets (20.9 × 7.9 nm^2) of SLGO (a, c, e) (~6 atom % O including in plane lattice vacancies (visible holes in the sheet) with O-containing functionalities and saturated, oxidized peripheral C atoms) and SLG (b, d, f) with the geometry calculated with the PM6/MOZYME method: (a, b) unfolded bands; (c, d) maximum folded structures corresponding to local minima on the potential energy surface (PES); (e) optimized SLGO structure (global minimum on PES); and (f) folded SLG structure (local minimum on PES, global minimum corresponds to the flat structure b).

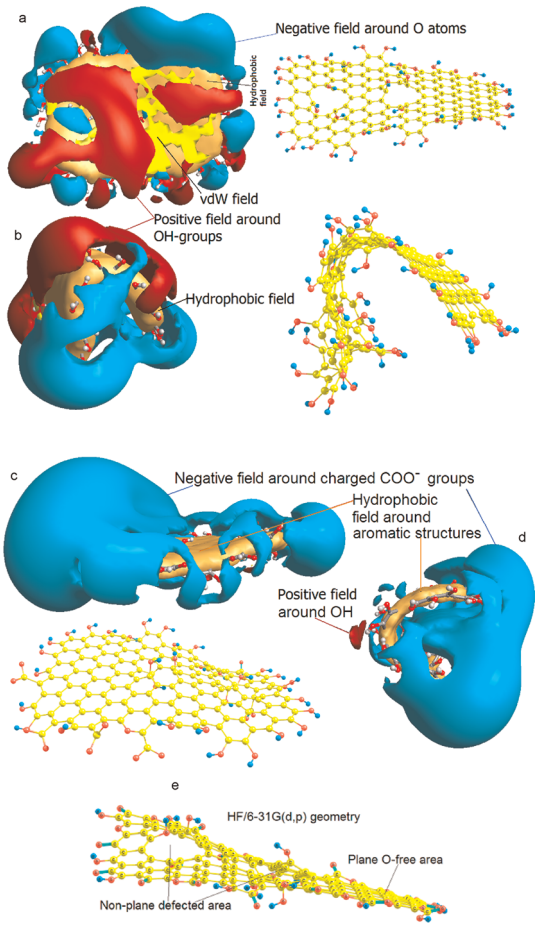

Figure 3. Scheme of the distribution of potential fields (red = positive, blue = negative, orange = hydrophobic, yellow = van der Waals, vdW calculated using FieldView 2.0.2) around a small SLGO sheet with zero total charge of (a) nonbent and (b) bent sheet and negatively charged sheet (c) nonbent and (d) bent; (e) *ab initio* HF/6-31G(d,p) calculation of the SLGO model showing two parts with planar O-free and nonplanar O-containing patches.

atoms or ions. In this visualization approach each atom or a group of atoms is considered as a "field point" of one of these four types, and together field points for a continuous field. For example, in a hydrophobic phenyl group the field point is at the center of the benzene ring. This approach has proved to be useful in analysis of crystal structures and drug discovery applications.[19]

There may be several possible mechanisms operating. First, each sheet has an uneven distribution of functional groups, which clustered around defect sites, particularly occupying lattice vacancies as terminating groups in addition to O-containing functionalities at the edges of the sheets. This still leaves certain unfunctionalized areas of "pure" graphene that also serve as sites for $\pi-\pi$ bond interactions (PM6/MOZYME), which correspond to the van der Waals (vdW) and hydrophobic fields around nonpolar fragments of the carbon sheets,[20] modeled in the FieldView studies. These sections of the SLGO sheet exhibit hydrophobic character (Figure 3a). Hydrophilic (positive and negative) fields are mainly located around O-containing functionalities and are much stronger at charged groups, for example, $-COO^-$ (Figure 3c,d). The hydrophilic field has a longer range ($\sim r^{-2}$ for charged groups) than vdW and hydrophobic fields ($\sim r^{-6}$) around unfunctionalized nonpolar areas. All conformation changes of SLGO in the aqueous environment are pH-dependent because of changes in the surface charge density around O-functionalities. These changes should lead to a reduction of the open area of the nonpolar fragments of folded sheets or sheet aggregates exposed to water.

The shapes of graphene sheet aggregates (envelope, star, rodlike, *etc.*)[13] observed in TEM images (Figure 1) depend on the pH at which the suspension was dried, given that conformational changes start in the aqueous medium and are enhanced during drying because of decreasing charging and electrostatic repulsive interactions that prevent aggregation of the sheets in the suspension. It has been calculated that bending occurs along lines with a maximal number of defects in the sheets (Figure 3b), which also results in a change of the distribution of different fields around the sheet, with contributions of both positive and negative hydrophilic fields increasing upon surface charging. The negative field in the inner space of the bent sheet, especially of a negatively charged sheet (Figure 3d), suggests that positively charged ions can be captured within bent SLGO structures.[13] Furthermore, *ab initio* HF/6-31G(d,p)[21] calculations reveal that the presence of lattice vacancies and the termination of the defect sites with O-containing groups also disrupt the planar geometry of graphene (Figure 3e). However, this slightly bent sheet remains unfolded because it is too small to be strongly bent or folded.

At low pH, O-functional groups of SLGO are fully protonated, and the hydrophobicity of the polycyclic aromatic network increases (Figure 3a, zones with vdW and hydrophobic fields increase, but zones with positive and negative fields decrease). This causes SLGO sheets to fold, stack, and precipitate out of solution. The final layered sample is dried at room temperature and it is possible that a hydration layer is still present between the layers of individual sheets maintaining a wider spacing (0.8 nm) between the graphene layers than the gap in the intrasheet-folded structure (0.3−0.4 nm). Multilayered aggregates of a complex geometry can contribute to the XRD peak at $2\theta \approx 11°$ (Supporting Information, Figure S4), for example, due to a smaller sheet (or its part) layered between two larger or incompletely overlapping sheets.

Herein, intersheet interactions dominate. As the pH increases, the negative surface charge on the oxygen-containing groups increases causing repulsion between neighboring sites. This implies that the number of oxygen-containing groups slightly differs on both sides of the graphene sheet, which would be

consistent with the initial acid-oxidation of the uppermost graphene layer while still apart of the graphite structure. Once detached, the introduction of additional oxygen-containing acidic groups due to acid-oxidation would proceed in other unfunctionalized areas, but would be unlikely to occur directly on the opposing site of an existing acid-functionalized area, otherwise etching would occur leading to a loss in the number of acidic groups rather than a gain.

The SLGO sheet would then bend away and fold allowing maximum separation of deprotonated sites (Supporting Information, Scheme S1). At the same time the folded structure reduces the exposure of unfunctionalized areas of the graphene layer to the aqueous environment due to a hydrophobic effect. At the edges, the separation of charged O-groups is restricted especially in highly oxidized SLGO. The SLGO sheet can collapse upon evaporation of the solvent,[22,23] causing the formation of nonplanar complex structures composed of many sheets. The existence of such a structure is reflected in the low temperature nitrogen adsorption−desorption isotherm, which has a long hysteresis loop (Supporting Information, Figure S5a, curve 1). As evaporation of water from basic solutions increases the concentration of the base, it drives the system toward high pH, the surface tension of the aqueous solution increases above that of water[24] causing greater contraction of the carbon nanomaterial system and providing a higher potential energy to drive the conformational changes. Even at neutral pH it can be seen that the charge distribution becomes less heterogeneous as the morphology of graphene changes from planar (Figure 3a) to a curved structure (Figure 3b). This may, in turn, lead to preferential arrangement of the sheets, which could explain the observed stacking during agglomeration or hierarchical ordering.[25] Collapse or stacking of the SLGO sheets also leads to a reduction in specific surface area (S_{BET}) and formation of voids, or pseudopores.

The S_{BET} value of 54 $m^2\ g^{-1}$ obtained for SLGO degassed at 150 °C prior to low temperature N_2 adsorption measurements (Supporting Information, Figure S5), is well below the theoretical value of 4200 or 2700 $m^2\ g^{-1}$ for small-sheet single or two to three layer graphene structures, respectively. This effect can be due to collapse of the sheets into relatively large and dense aggregates of a complex structure. The low S_{BET} for heated SLGO is close to that of exfoliated graphite (20 $m^2\ g^{-1}$) with stacks of 100−200 nm in thickness. However, the texture of heated SLGO and exfoliated graphite are markedly different because pores with very complex geometry were formed within the crumpled flexible SLGO sheets on degassing, similar to the structures observed in TEM images (*e.g.*, Figure 1a,c). The crumpling of individual graphene sheets needs much less energy than the crumpling of multilayer structures of exfoliated graphite.

Conformational changes induced in SLGO with ~6 atom % O were calculated using molecular dynamic (MD) simulations (Supporting Information, Figure S6). Calculations were done for larger (20.9 × 7.9 nm^2) and smaller (20.8 × 3.9 nm^2) graphene sheets. The geometry of initially hydrated folded SLGO structures was optimized using molecular mechanics (MM) with the same force field (Figure S6a,f). Rapid drying of SLGO at 150 °C used for degassing of samples was simulated with the MD method for 10−30 ps (enough to obtain significant changes in the geometry of the systems with MD operating with the average temperature −molecular velocity relationship). The heating caused a smaller sheet to unfold and water molecules scatter in a large volume (Figure S6b,c). However, drying at lower temperatures slows the unfolding process at 0 °C and induces flattening of the SLGO structure when cooled to −73 °C (Figure S6d,e). A larger SLGO sheet (Figure 2a,c) in a hydrated state (Figure S6f) remains folded at heating to 150 °C for 20 ps (Figure S6g). Despite removal of water upon heating, this bent structure remains folded due to stronger attractive hydrogen bonding of hydroxyls and other O-containing functionalities and dispersion interactions between nonpolar fragments of larger bent structures. This result of MD simulations is in agreement with TEM images obtained for dried SLGO with collapsed structures. The Raman spectra (Figure S7) show that aggregation and crumpling of SLGO sheets upon degassing does not result in graphitization of the sample despite the strong reduction of S_{BET}. Thus, the presence of a significant number of O-containing functionalities in SLGO controls the graphitic motifs in its structure even after heating and collapse of its "free" sheets.

CONCLUSIONS

SLGO in the wet state, dried from the wet state, and in the dry state exhibits very different textural characteristics that are governed by the chemical environment, in particular pH, as well as its oxygen-containing functional groups and their surface charge. At basic pH SLGO sheets tend to fold owing to the electrostatic repulsion between negatively charged deprotonated acidic groups, and SLGO suspensions are stable, whereas at low pH SLGO suspensions are destabilized owing to stronger intersheet interactions and higher zeta-potential. Upon drying, SLGO sheets form dense aggregates with complex structure and porosity, and low BET surface area. Depending on the geometric size of SLGO sheets and drying conditions, they can unfold or remain folded due to hydrogen bonding between polar surface functional groups and dispersion interactions between nonpolar graphene fragments.

Therein careful selection of the chemical environment and the surface functionality and reactivity of single-layer graphene oxide sheets is required when tailoring SLGO for specific applications.

METHODS

SLGO Folding. SLGO was purchased from CheapTubes Inc., washed extensively in water and methanol, and subsequently dried from acetone under a vacuum in order to remove any possible residual chemicals from their synthesis method. SLGO was placed in 2 M NaOH solution and sonicated for 30 min and left for 24 h. SLGO was subsequently separated *via* centrifugation and washing with pure water, but no fulvic acids (oxidative debris) were eluted from the SLGO. The surface oxygen-containing groups were regenerated in 0.1 M HCl on stirring for 4 h and then separated *via* centrifugation and washing with pure water. SLGO (50 mg) was dispersed in either hydrochloric acid (pH 1) or sodium hydroxide (pH 12) or 10 mM buffered solutions of acetic acid/ammonium acetate (pH 5), sodium dihydrogenphosphate/disodium hydrogenphosphate (pH 7), or ammonium hydroxide/ammonium chloride (pH 9). Small drops were taken from the resulting dispersion, dropped onto TEM grids, and allowed to dry.

Potentiometric Titration Analysis. For purification, the precipitated SLGO sample was centrifuged, the supernatant was discarded, and the sediment was washed with Millipore water until its dispersion. Then the dispersed SLGO was precipitated by adding 1 M HCl with constant stirring to pH ≈ 1.0, and the suspension was allowed to stand for some hours. The precipitated sample was centrifuged, and the supernatant was discarded, and the sediment was diluted with some water, washed until negative chloride test with $AgNO_3$ solution was obtained, and then freeze-dried (all evaporable components escaped). Equilibrium titration employed a self-developed titration system (GIMET1), 665 Dosimat (Metrohm) burets, a magnetic stirrer, a high performance potentiometer, a pH electrode (OP-0808P Radelkis), and an IBM PS/1 PC. A CO_2-free condition was provided by nitrogen bubbling. The measuring system was calibrated both for pH and for H^+/OH^- ion concentration. Three buffer solutions (Radelkis, Hungary) were used to check the Nernstian response of the pH electrode. The experimental activity coefficients of H^+/OH^- ions were determined from the background electrolyte titration at each ionic strength. The evaluation of titration data was based on the calculation of the material balance for H^+/OH^- ions. Titration was carried out using HCl and KOH solutions from pH ~3 to ~10 (8258 s), and back from pH ~10 to ~3 (4196 s) with varied KCl concentration.

Zeta Potential. Electrophoretic mobility (U_e) of SLGO particles (15 mg of SLGO per 30 mL of of Milli-Q water) was measured at 25 °C in a disposable zeta cell (DTS 1060) using a NanoZS (Malvern, UK) apparatus. The pH values were adjusted by the addition of HCl or NaOH solutions, and the salinity was changed by the addition of NaCl (0.01 M). Zeta potential (ζ) was calculated from the mobility using the Smoluchowski equation. According to the Smoluchowski theory,[26] there is a linear relationship between the U_e and ζ values: $U_e = A\zeta$, where A is a constant for a thin electrical double layer at $\kappa a \gg 1$ (where a denotes the particle radius, and κ is the Debye–Huckel parameter).

Molecular Simulations. Molecular dynamic (MD) simulations of SLG and SLGO models (carbon sheets with ~3300 to 7000 atoms of 81.4–165.3 nm^2 in size and in a hydrated state with ~6200–13000 atoms) were made using the CharMM force field (VEGA ZZ, version 2.4[27] with NAMD 2.7b3[28]). The MD calculations were used to analyze the temperature effects on the dynamic changes of hydrated SLGO sheets (details are shown in the ESI). Quantum chemical calculations of the SLG (6146 atoms with no O atoms) and SLGO (6357 atoms with ~6 at% of O atoms) models were carried out using semi-empirical method PM6 (MOPAC 2009, versions 10.341 L and 11.038 L with the MOZYME algorithm).[15] The O-containing groups totally covered the graphene edges and a portion of the O atoms in the form of different groups (COH, COOH, C=O, C–O–C) was attached to C atoms in the inner-sheet defects[29] randomly distributed in the sheets. *Ab initio* calculations (Gaussian 03[21] with HF/6-31G(d,p) basis set) of the geometry of relatively small models (~220 atoms) of SLGO were performed (without consideration of the solvation effects) to show the oxidizing effects on the bending of the SLGO sheets. Simple but pictorial calculations of potential fields (positive, negative, hydrophobic, van der Waals, vdW) with the FieldView 2.0.2 program are described in detail elsewhere.[30] The *ab initio* method was used to analyze the oxidizing effects on the geometry (bending) of relatively small fragments (~220 atoms) of SLG and SLGO. The PM6 method was used to study certain geometric features of relatively large SLG and SLGO sheets. The MD method was used to study the bending/folding/unfolding and temperature effects of hydrated SLGO (up to 13000 atoms). The initial geometry of the SLGO and SLG sheets was both flat and strongly bent, and then it was optimized within all the used methods.

Conflict of Interest: The authors declare no competing financial interest.

Acknowledgment. We thank the EC Seventh Framework Programme (FP7/2007-2013), Marie Curie International Research Staff Exchange Scheme (COMPOSITUM, Grant No. 230790), Marie-Curie Industry-Academia Partnerships and Pathways Programme (PIAP-GA-2009-251429 UNCOS, PIAP-GA-2008-230676 CARBOSORB), and the RCUK Academic Fellowship Scheme for financial support and L. Radovic, Penn State University, USA, for useful discussions.

Supporting Information Available: Additional results for the zeta potential, TEM, TGA, powder XRD, liquid nitrogen adsorption, MD (CharMM force field) simulations, schematic of the conformational changes of graphenes and Raman spectroscopy. This material is available free of charge *via* the Internet at http://pubs.acs.org.

REFERENCES AND NOTES

1. Satti, A.; Larpent, P.; Gun'ko, Y. Improvement of Mechanical Properties of Graphene Oxide/Poly(allylamine) Composites by Chemical Crosslinking. *Carbon* **2010**, *48*, 3376–3381.
2. Voitko, K. V.; Whitby, R. L. D.; Gun'ko, V. M.; Bakalinska, O. M.; Kartel, M. T.; Laszlo, K.; Cundy, A. B.; Mikhalovsky, S. V. Morphological and Chemical Features of Nano and Macroscale Carbons Affecting Hydrogen Peroxide Decomposition in Aqueous Media. *J. Colloid Interface Sci.* **2011**, *361*, 129–136.
3. Kim, K.; Lee, Z.; Malone, B.; Chan, K. T.; Alemán, B.; Regan, W.; Gannett, W.; Crommie, M. F.; Cohen, M. L.; Zettl, A. Multiply Folded Graphene: Grafold. *Phys. Rev. B* **2011**, *83*, 245433.
4. Liu, Z.; Robinson, J. T.; Sun, X.; Dai, H. PEGylated Nanographene Oxide for Delivery of Water-Insoluble Cancer Drugs. *J. Am. Chem. Soc.* **2008**, *130*, 10876–10877.
5. Sreeprasad, T. S.; Maliyekkal, S. M.; Lisha, K. P.; Pradeep, T. Reduced Graphene Oxide-Metal/Metal Oxide Composites: Facile Synthesis and Application in Water Purification. *J. Hazard. Mater.* **2011**, *186*, 921–931.
6. Zhang, J.; Xiao, J.; Meng, X.; Monroe, C.; Huang, Y.; Zuo, J.-M. Free Folding of Suspended Graphene Sheets by Random Mechanical Stimulation. *Phys. Rev. Lett.* **2010**, *104*, 166805.
7. Pandey, D. K.; Chung, T. F.; Prakash, G.; Piner, R.; Chen, Y. P.; Reifenberger, R. Folding and Cracking of Graphene Oxide Sheets upon Deposition. *Surf. Sci.* **2011**, *605*, 1669–1675.
8. Fogler, M. M.; Castro Neto, A. H.; Guinea, F. Effect of External Conditions on the Structure of Scrolled Graphene Edges. *Phys. Rev. B* **2010**, *81*, 161408(R).

9. Singh, V.; Joung, D.; Zhai, L.; Das, S.; Khondaker, S. I.; Seal, S. Graphene Based Materials: Past, Present and Future. *Prog. Mater. Sci.* **2011**, *56*, 1178–1271.
10. Xu, Z. P.; Buehler, M. J. Geometry Controls Conformation of Graphene Sheets: Membranes, Ribbons, and Scrolls. *ACS Nano* **2010**, *4*, 3869–3876.
11. Li, D.; Muller, M. B.; Gilje, S.; Kaner, R. B.; Wallace, G. G. Processable Aqueous Dispersions of Graphene Nanosheets. *Nat. Nanotechnol.* **2008**, *3*, 101–105.
12. Shih, C.-J.; Lin, S.; Sharma, R.; Strano, M. S.; Blankschtein, D. Understanding the pH-Dependent Behavior of Graphene Oxide Aqueous Solutions: A Comparative Experimental and Molecular Dynamics Simulation Study. *Langmuir* **2012**, *28*, 235–241.
13. Whitby, R. L. D.; Korobeinyk, A.; Gun'ko, V. M.; Busquets, R.; Cundy, A. B.; Laszlo, K.; Skubiszewska-Zięba, J.; Leboda, R.; Tombacz, E.; Toth, I. Y.; *et al*. pH-Driven Physicochemical Conformational Changes of Single-Layer Graphene Oxide. *Chem. Commun.* **2011**, *47*, 9645–9647.
14. Futaba, D. N.; Hata, K.; Yamada, T.; Hiraoka, T.; Hayamizu, Y.; Kakudate, Y.; Tanaike, O.; Hatori, H.; Yumura, M.; Iijima, S. Shape-Engineerable and Highly Densely Packed Single-Walled Carbon Nanotubes and Their Application as Super-Capacitor Electrodes. *Nat. Mater.* **2006**, *5*, 987–994.
15. Stewart, J. J. P. *MOPAC2009*; Stewart Computational Chemistry: Colorado Springs, CO, 2008; http://openmopac.net/.
16. Whitby, R. L. D.; Korobeinyk, A.; Glevatska, K. V. Morphological Changes and Covalent Reactivity Assessment of Single-Layer Graphene Oxides under Carboxylic Group-Targeted Chemistry. *Carbon* **2011**, *49*, 722–725.
17. Gomez-Navarro, C.; Weitz, R. T.; Bittner, A. M.; Scolari, M.; Mews, A.; Burghard, M.; Kern, K. Electronic Transport Properties of Individual Chemically Reduced Graphene Oxide Sheets. *Nano Lett.* **2007**, *7*, 3499–3503.
18. Rose, S.; Vinter, A. Molecular Field Technology and Its Applications in Drug Discovery. *Innovations Pharm. Technol.* **2007**, *23*, 14–18.
19. Sandeman, S. R.; Gun'ko, V. M.; Bakalinska, O. M.; Howell, C. A.; Zheng, Y.; Kartel, M. T.; Phillips, G. J.; Mikhalovsky, S. V. Adsorption of Anionic and Cationic Dyes by Activated Carbons, PVA Hydrogels, and PVA/AC Composite. *J. Colloid Interface Sci.* **2011**, *358*, 582–592.
20. Cheeseright, T.; Mackey, M.; Rose, S.; Vinter, A. Molecular Field Extrema as Descriptors of Biological Activity: Definition and Validation. *J. Chem. Info. Model.* **2006**, *46*, 665–676.
21. Frisch, M. J.; Trucks, G. W.; Schlegel, H. B.; Scuseria, G. E.; Robb, M. A.; Cheeseman, J. R.; Scalmani, G.; Barone, V.; Mennucci, B.; Petersson, G. A.; *et al*., *Gaussian*; Gaussian Inc.: Wallingford, CT, 2004.
22. Gao, Y.; Chen, X. Q.; Xu, H.; Zou, Y. L.; Gu, R. P.; Xu, M. S.; Jen, A. K. Y.; Chen, H. Z. Highly-Efficient Fabrication of Nanoscrolls from Functionalized Graphene Oxide by Langmuir-Blodgett Method. *Carbon* **2010**, *48*, 4475–4482.
23. Xie, X.; Ju, L.; Feng, X. F.; Sun, Y. H.; Zhou, R. F.; Liu, K.; Fan, S. S.; Li, Q. L.; Jiang, K. L. Controlled Fabrication of High-Quality Carbon Nanoscrolls from Monolayer Graphene. *Nano Lett.* **2009**, *9*, 2565–2570.
24. Myers, D., *Surfactant Science and Technology*, 3rd ed.; Wiley-VCH: New York, 2005.
25. Yin, S.; Zhang, Y.; Kong, J.; Zou, C.; Li, C. M.; Lu, X.; Ma, J.; Boey, F. Y. C.; Chen, X. Assembly of Graphene Sheets into Hierarchical Structures for High-Performance Energy Storage. *ACS Nano* **2011**, *5*, 3831–3838.
26. Hunter, R. J. *Zeta Potential in Colloid Sciences*; Academic Press: London, 1981.
27. Pedretti, A.; Villa, L.; Vistoli, G. VEGA—An Open Platform to Develop Chemo-Bio-Informatics Applications, Using Plug-In Architecture and Script Programming. *J. Comput.-Aided Mol. Des.* **2004**, *18*, 167–173.
28. Phillips, J. C.; Braun, R.; Wang, W.; Gumbart, J.; Tajkhorshid, E.; Villa, E.; Chipot, C.; Skeel, R. D.; Kale, L.; Schulten, K. Scalable Molecular Dynamics with NAMD. *J. Comput. Chem.* **2005**, *26*, 1781–1802.
29. FieldView 2.0.2, www.cresset-group.com, (Accessed September 12, 2011).